NASA/TM-20260007877

A Dispersion-Strengthened Low-Density Niobium Alloy and Its Elevated Temperature Mechanical Performance

Eric Brizes, Timothy Smith, Christopher Kantzos, Justin Milner, and Rebekah Webster
Glenn Research Center, Cleveland, Ohio

Aurelia Moriyama-Gurish
Yale University, New Haven, Connecticut

Doyle Weishar
University of Virginia, Charlottesville, Virginia

September 2026

NASA STI Program Report Series

Since its founding, NASA has been dedicated to the advancement of aeronautics and space science. The NASA scientific and technical information (STI) program plays a key part in helping NASA maintain this important role.

The NASA STI program operates under the auspices of the Agency Chief Information Officer. It collects, organizes, provides for archiving, and disseminates NASA's STI. The NASA STI program provides access to the NTRS Registered and its public interface, the NASA Technical Reports Server, thus providing one of the largest collections of aeronautical and space science STI in the world. Results are published in both non-NASA channels and by NASA in the NASA STI Report Series, which includes the following report types:

- TECHNICAL PUBLICATION.
  Reports of completed research or a major significant phase of research that present the results of NASA programs and include extensive data or theoretical analysis. Includes compilations of significant scientific and technical data and information deemed to be of continuing reference value. NASA counterpart of peer-reviewed formal professional papers but has less stringent limitations on manuscript length and extent of graphic presentations.

- TECHNICAL MEMORANDUM.
  Scientific and technical findings that are preliminary or of specialized interest, e.g., quick release reports, working papers, and bibliographies that contain minimal annotation. Does not contain extensive analysis.

- CONTRACTOR REPORT.
  Scientific and technical findings by NASA-sponsored contractors and grantees.

- CONFERENCE PUBLICATION.
  Collected papers from scientific and technical conferences, symposia, seminars, or other meetings sponsored or cosponsored by NASA.

- SPECIAL PUBLICATION.
  Scientific, technical, or historical information from NASA programs, projects, and missions, often concerned with subjects having substantial public interest.

- TECHNICAL TRANSLATION.
  English-language translations of foreign scientific and technical material pertinent to NASA's mission.

Specialized services also include organizing and publishing research results, distributing specialized research announcements and feeds, providing information desk and personal search support, and enabling data exchange services.

For more information about the NASA STI program, see the following:

- Access the NASA STI program home page at http://www.sti.nasa.gov

NASA/TM-20260007877

A Dispersion-Strengthened Low-Density Niobium Alloy and Its Elevated Temperature Mechanical Performance

Eric Brizes, Timothy Smith, Christopher Kantzos, Justin Milner, and Rebekah Webster
Glenn Research Center, Cleveland, Ohio

Aurelia Moriyama-Gurish
Yale University, New Haven, Connecticut

Doyle Weishar
University of Virginia, Charlottesville, Virginia

National Aeronautics and
Space Administration

Glenn Research Center
Cleveland, Ohio 44135

September 2026

Acknowledgments

The high-temperature alloy research performed in this work at NASA Glenn Research Center was funded by the Internal Research and Development (IRAD) Enabling Niobium-based Alloy and Coating Technologies (ENACT) project. This work was made possible through the assistance of multiple staff members and visiting students in NASA Glenn Research Center's Advanced Metallics Branch and Environmental Effects and Coatings Branch. We would like to acknowledge the technical inputs from Aaron Thompson, Erin Falkosky, Dr. Bryan Harder, Dr. Elizabeth Young-Dohe, and Dr. Ronald Noebe to the additive manufacturing, mechanical testing, preparation of samples, and the electron microscopy conducted.

Level of Review: This material has been technically reviewed by technical management.

This report is available in electronic form at https://www.sti.nasa.gov/ and https://ntrs.nasa.gov/

NASA STI Program/Mail Stop 050
NASA Langley Research Center
Hampton, VA 23681-2199

A Dispersion-Strengthened Low-Density Niobium Alloy and Its Elevated Temperature Mechanical Performance

Eric Brizes, Timothy Smith, Christopher Kantzos, Justin Milner, and Rebekah Webster
National Aeronautics and Space Administration
Glenn Research Center
Cleveland, Ohio 44135

Aurelia Moriyama-Gurish
Yale University
New Haven, Connecticut 06511

Doyle Weishar
University of Virginia
Charlottesville, Virginia 22904

Abstract

In response to the elevated-temperature and weight-reduction demands of modern aerospace applications, a novel oxide-dispersion-strengthened low-density niobium alloy (LDNb-ODS) was fabricated using laser powder bed fusion (L-PBF). To overcome powder procurement barriers, L-PBF feedstock was produced by blending commercial Nb521, Ti64, and Cr powder with Y_2O_3 nanoparticles via resonant acoustic mixing. Following L-PBF and a 1,400 °C vacuum heat treatment, the alloy achieved a density of 6.73 g/cc and a fine mean grain size of 4.62 µm stabilized by uniform ~30 nm yttria dispersoids. Microstructural analysis revealed a chemically inhomogeneous build with lack-of-fusion defects and a titanium (Ti) shift from a nominal 31.5 wt% in the starting powder blend to 24.8 wt% in the printed part due to preferential Ti loss during printing. Elevated-temperature tensile testing demonstrated that LDNb-ODS maintained a superior specific yield strength of 60 to 85 MPa/(g/cc) up to 800 °C, outperforming nickel-based alloys Ni625, Ni230, and GRX-810. Between 870 and 950 °C, its specific strength surpassed both Ni718 and Ni625. In rapid stress-rupture testing at 1,093 °C and 20.7 MPa, uncoated LDNb-ODS survived 21.4 hr (a tenfold increase over legacy C-103) while an R512E silicide coating extended rupture life to 84.8 hr, confirming that oxidation accelerates low-stress failure. These findings demonstrate that additive manufacturing of LDNb-ODS provides a viable, lightweight alternative to nickel-based superalloys for high-temperature (>850 °C) aerospace components.

Abbreviations

AM	additive manufacturing
APS	average particle size
ASTM	American Society for Testing and Materials
BCC	body-centered cubic
BSE	backscattered electron
EDM	electrical discharge machining
EDS	energy dispersive spectroscopy
ETMT	electro-thermal mechanical testing
FEG-SEM	field emission gun scanning electron microscope

GRC	Glenn Research Center (NASA)
L-PBF	laser powder bed fusion
LDNb	low-density niobium
NASA	National Aeronautics and Space Administration
ODS	oxide dispersion strengthened / oxide dispersion strengthening
PSD	particle size distribution
SE	secondary electron
SEM	scanning electron microscopy
UHP	ultra-high purity
UTS	ultimate tensile strength
VHT	vacuum heat treatment
YS	0.2% offset yield strength

1.0 Introduction

Niobium-based alloy development increased rapidly during the late 1950s and 1960s, driven by the high-temperature requirements of aerospace and space nuclear power applications (Ref. 1). This material class experienced unprecedented growth because breakthroughs in refractory metal processing (such as electron beam smelting and refining) aligned with the engineering demands of early space exploration (Ref. 2). Niobium (Nb) alloys are uniquely suited for these applications because they are the least dense of the refractory metals. They also have excellent room-temperature ductility, demonstrate good weldability, and can be readily fabricated into thin sheets and complex structural shapes (Refs. 3 to 4). Because of these traits, Nb alloys became the preferred materials for structural components and thermal protection systems in high-speed aircraft, spacecraft, satellites, and low-altitude rockets (Refs. 3 and 5). Early Nb alloy development in the United States focused on two main goals: improving creep resistance and overcoming catastrophic high-temperature oxidation. Unalloyed Nb oxidizes rapidly above 500 °C in air. It undergoes a transition to rapid linear kinetics as the oxide scale cracks and spalls under high compressive growth stresses (Refs. 6 and 7).

Prior to 1960, researchers believed that adding aluminum to Nb caused extreme processing difficulties, reporting that aluminum-containing alloys were virtually unworkable (Ref. 8). However, this view changed when Wlodek et al. (Union Carbide Corp., Niagara Falls, NY) demonstrated that Nb-based alloys containing 0 to 40 wt% titanium (Ti), 0.5-10 wt% vanadium (V) or chromium (Cr), and 0.5 to 10 wt% aluminum (Al) could combine reliable workability with high-temperature strength and oxidation resistance above 1,000 °C (Refs. 9). Their efforts showed how these alloys could be fabricated by non-consumable arc-melting under inert atmospheres and then shaped by extrusion, rolling, or swaging. The Ti, Al, and V or Cr additions dramatically suppressed oxidation rates. At 1,000 °C in pure oxygen, these alloys gained only 50 mg/cm² after 100 hr, compared to a 6670 mg/cm² weight gain for unalloyed Nb under identical conditions (Refs. 9). This work founded the low-density Nb (LDNb) alloy family, which in essence are Nb-based yet heavily alloyed with Ti, Al, and Cr and/or V to reduce density and improve oxidation resistance.

In general, alloying additions improve the oxidation resistance of Nb by changing the properties and growth kinetics of the oxide scale. One main mechanism lowers the oxidation rate by modifying the atomic structure of the unprotective Nb_2O_5 oxide that readily forms on Nb alloys. Elements with higher valences and oxygen affinities, like Mo and W, dissolve into the oxide to fill oxygen vacancies and reduce anion defects. Adding elements with smaller atomic radii than Nb, such as Ti, Cr, V, and Al, decreases the lattice parameter of the scale; lowering the oxide-to-metal volume ratio, which prevents

scale spallation (flaking) and improves mechanical stability (Refs. 10). Ti and Al also form oxides with lower free energies of formation than Nb_2O_5 and have stable Pilling-Bedford Ratios between 1.0 and 2.0, making the scale less likely to buckle. Additionally, Cr, V, and Ti reduce oxidation by lowering both the solubility and the diffusion coefficient of oxygen within the underlying alloy matrix (Refs. 10). However, the most effective way to reduce oxidation is to form alternative, slower-growing protective oxides instead of Nb_2O_5. Elements with high oxide free energies of formation, like Cr at concentrations over 30 wt%, preferentially oxidize to form a chromia protective external scale instead of causing internal oxidation. Complex mixed oxides also provide excellent protection. For example, adding more than 6 at% Ti forms a mixed oxide (TiO_2+Nb_2O_5), and maximum oxidation resistance occurs at Ti levels of 20 to 40 wt% (Ref. 10). Alloying can also completely destabilize the porous and unfavorable Nb_2O_5 phase. Small amounts of V (~3 wt%) used together with Al promote the formation of more protective NbO and NbO_2 suboxides (Ref. 10).

With this understanding, Wlodek et al. identified optimal alloy chemistries within the ranges of 5-20 Ti, 3-12 Cr, 2-6 Al, and 1-5 V (wt%). These specific chemical compositions formed an adherent, non-volatile oxide scale that resisted oxidation at temperatures above 1,100 °C. Their patented Nb-20Ti-10Cr-4Al-4V (wt%) alloy modified with 5 wt% iron (Fe) or nickel (Ni) achieved remarkably low 100-hr weight gains of just 32.4 to 48.1 mg/cm² at 1,000 °C and 132.0 to 189.4 mg/cm² at 1,200 °C (Ref. 9). Despite these benefits, engineers noted that high Ti contents significantly reduced the alloy's melting temperature, high-temperature strength, and creep resistance. And because efforts in the 1960s focused mostly on increasing high-temperature mechanical performance, several major programs stopped researching low-density, Ti- and Al-containing Nb alloys (Ref. 8).

Research on high-temperature structural Nb alloys abruptly ended in the US in the early 1970s due to policy changes and a sharp drop in NASA funding. The U.S. also stopped working on space-based nuclear power systems in 1973 and chose reusable ceramic tiles instead of coated refractory metals for the Space Shuttle's thermal protection (Refs. 2 and 10). Because of this, Nb alloy development ceased in the U.S. for decades, leaving American engineers to rely on the state-of-the-art alloys of 1974 (Ref. 10).

Meanwhile, the Soviet Union's refractory metal program continued through the 1970s and 1980s until the Soviet Union dissolved in 1991. Their steady work led to advancements in processable dispersion-strengthened Nb alloys (Refs. 11 and 12). As US efforts stalled and Soviet programs matured, distinct Nb alloy tiers based on strength vs. workability emerged, totaling over 20 unique alloy designations, such as C-103, Cb-752, and FS-85 developed in the United States and VN-7 and 5VMTs developed in the Soviet Union (Refs. 3 and 4). The American alloys relied primarily on tungsten (W) and hafnium (Hf) as solid-solution strengthening elements, while the Soviet variants favored combinations of molybdenum (Mo), and zirconium (Zr). Both used fine carbide or complex carbonitride dispersions (0.05-0.45 C or N, wt%) as a secondary phase strengthening mechanism to enhance creep resistance (Refs. 4 and 13). However, none of these mature alloys included significant amounts of Ti, Cr, or Al and thus they do not fall within the LDNb alloy family.

In the early 1980s, Soviet researchers started developing LDNb alloy sheet materials. They understood that alloying Nb with large quantities of Ti improves its oxidation resistance but sharply reduces high-temperature strength, particularly above 1,000 °C (Ref. 14). In an attempt to overcome this deficiency, they clad a high-strength core of the 5VMTs alloy (Nb-5W-2Mo-1Zr, wt%) with oxidation-resistant, cold-formable VN-7 low-density alloy layers (Nb-41Ti-5Al, wt%). Mechanical evaluations revealed that the VN-7 clad 5VMTs sheet had superior short-term tensile properties up to 1,300 °C. However, its stress-rupture strength was inferior to unclad 5VMTs in the 1,000 to 1,400 °C range (Ref. 14). The loss in stress-rupture performance was driven by Ti diffusion during high-temperature

testing. Specifically, Ti within the VN-7 cladding diffused into the 5VMTs core, which lowered the melting range and high-temperature strength of the core.

Shortly after, O.I. Eliseeva et al. characterized the relationship between mechanical properties, heat treatment, and phase composition in the Soviet alloy VN-10 (Nb-30Ti-7Al-5Mo-4Cr-0.05C, wt%) (Ref. 15). Note that the VN-10 alloy designation represents a range of chemical compositions surrounding ~Nb-31Ti-7Al-4V-1.5Zr-0.08C (wt%) and therefore may differ between publications. Designed as a low-density, oxidation-resistant material for gas turbine engine compressor blades operating up to 700 to 750 °C, VN-10 uses carbon additions to create a carbide-strengthened microstructure. VN-10 exhibits high room-temperature tensile strengths of 1,100 to 1,700 MPa. This strength decreases rapidly to ~700 MPa upon heating to 300 °C but is then maintained up to ~800 °C (Ref. 15).

In 1984, the US renewed refractory metal research, but at a much lower level. This revival was driven by a reconsideration of compact space nuclear power systems and the start of the Integrated High Performance Turbine Engine Technology (IHPTET) and National Aerospace Plane (NASP) propulsion programs (Ref. 10). These programs required materials with both high specific strength and elevated-temperature environmental stability up to 1,500 °C to reduce component cooling and increase system efficiency. Melvin R. Jackson (*General Electric Co.*, Schenectady, NY) led an effort to develop lightweight structural alloys for aircraft engines. To map the Nb-Ti alloy space, Jackson collaborated with Karen D. Jones, a graduate student from the *Rensselaer Polytechnic Institute*. Her 1990 Master's thesis summarizes the technical foundation for this work (Ref. 10). Jackson and Jones characterized the microstructure, evaluated mechanical performance, and conducted environmental testing of Nb-Ti-based (i.e., LDNb) alloys. Their work showed that precise additions of Al and Cr maintained a ductile body-centered cubic (BCC) crystal structure, delayed oxygen embrittlement, and increased the uncoated use-temperature by 200 to 400 °C compared to standard commercial Nb alloys like C-103 and Cb-752 (Ref. 10).

Jackson and *General Electric* later patented these LDNb alloys. The patented family included a wide range of Ti, Al, Cr, and Hf to keep densities between 5.8 and 6.7 g/cc, providing a 20% to 25% weight reduction compared to Ni-base superalloys (Ref. 16). The patented compositions are defined in atomic percent (at%) by the expression: $Nb\text{-}Ti_{27\text{-}40.5}\text{-}Al_{4.5\text{-}10.5}\text{-}Hf_{1.5\text{-}5.5}\text{-}Cr_{4.5\text{-}7.9}\text{-}V_{0\text{-}6}$ where the Ti/Nb atomic ratio is constrained to $Ti/Nb > 0.5$ to ensure oxidation resistance and $10.5 < Hf + V + Al + Cr < 16.5 + (5 * Ti/Nb)$ to maintain room-temperature ductility and cold workability (Ref. 16). Within these boundaries, individual element levels are restricted to 4.5-10.5 Al, 1.5-5.5 Hf, 4.5-7.9 Cr, and 0-6 V (at%) to prevent brittle intermetallic phases from forming. Jackson also showed that the Ti/Nb ratio strongly influences the elevated temperature mechanical strength. Alloys were prepared with Ti/Nb ratios ranging from 0.5 to 0.9. While some alloys had similar room-temperature tensile strengths, their high-temperature performance differed significantly. At 980 °C, the alloy with a Ti/Nb ratio of 0.5 (lower Ti, ~15-20 wt%) was 1.5 times stronger than the alloy with a Ti/Nb ratio of 0.9 (higher Ti, ~25-30 wt%). At 1,200 °C, it was nearly 3 times stronger. To restrict grain growth during high-temperature manufacturing and service, they added 0-1 Zr and 0-0.5 C (at%) (Ref. 16). And to test workability, they cold-rolled multiple alloy sheets (achieving a 50% reduction between 1,000 to 1,100 °C anneals) and successfully bent a 0.75 mm thick sheet 90° around a 1.5 mm radius mandrel.

To transition from the laboratory to commercial products, a series of studies focused on optimizing LDNb alloy compositions and scaling up production (Refs. 17 to 20). Vinod K. Sikka (Oak Ridge National Laboratory, Oak Ridge, TN) and Edward A. Loria (Niobium Products Co. (CBMM), Corapolis, PA) investigated a multi-component alloy with the nominal composition 44Nb-35Ti-6Al-5Cr-8V-1W-0.5Mo-0.3Hf (at%), or Nb-24.3Ti-2.4Al-3.8Cr-5.9V-2.7W-0.7Mo-0.8Hf in wt%, produced via industrial-scale practices (Refs. 21 and 22). This composition limits the total alloying content to maintain a fully BCC microstructure. It uses W and Mo to maximize lattice misfit solid-solution strengthening and creep

resistance. Additionally, the alloy incorporates Hf as an interstitial scavenger and to prevent grain coarsening, along with Al, Cr, and V for oxidation resistance without inducing room-temperature brittleness (Refs. 23).

To produce the alloy, the researchers used powder metallurgy to mix and press raw materials into disks. These disks were then double-plasma-arc cold-hearth melted to produce a 73.5 kg ingot measuring 15.3 cm in diameter and 61.0 cm in length. Following initial extrusion to an 8.13 cm diameter, a segment of the ingot was sequentially re-extruded, cold-swaged, and annealed down to a 1.6 cm (0.625 in.) diameter bar. This process yielded a uniform grain size of 22 to 25 μm (Refs. 21 and 22).

Tensile testing of the processed 1.6 cm bar in air at room temperature resulted in a 1,107 MPa yield strength, a 1,117 MPa ultimate tensile strength, and a 16.2% elongation. However, testing in air at elevated temperatures (above 700 °C) caused embrittlement. Elongation dropped to a minimum of 1.8%, and the fracture mode changed from ductile dimple to intergranular fracture. In contrast, tests conducted in a vacuum at 750 and 850 °C restored ductility. These vacuum tests yielded elongations of 26.8% and 36.0%, respectively, and showed ductile dimple fracture modes (Ref. 21). This proved that the high-temperature ductility loss was caused by oxygen embrittlement, which must be mitigated with protective coatings in practical applications.

The Chinese aerospace sector prioritized research into LDNb alloys in the 2000s (Refs. 5 and 24). Institutions like the Northwest Institute for Nonferrous Metal Research (NIN), Ningxia Orient Tantalum Industry Company (OTIC), Central South University, Northwestern Polytechnical University, and Nanjing University of Aeronautics and Astronautics led the way. Together, Chinese researchers systematically benchmarked a wide variety of Western and Soviet structural alloys and environmental barrier coatings (Refs. 2 and 24). They explored processing methodologies such as electron beam melting, hot isostatic pressing, and vacuum arc melting. Through these methods, they successfully produced large-scale, LDNb alloy plates exceeding 500 mm in width with densities less than 6 g/cc.

Primary LDNb product series include the Nb-31Ti-7Al-xV-1.5Zr (x=3-10, wt%) sheet alloy developed by NIN for cold-stamped rings, and the Nb-35Ti-6Al-xCr-yV-1W-0.5Zr (x=2-10, y=3-8, wt%) structural bar alloy (Refs. 5 and 13). Parallel work focused on microalloying techniques and grain refinement through interstitial additions in the Nb-Ti-Al-Cr and Nb-Ti-Al-Zr systems to establish scalable routes for fine-grained large diameter structural bar (Ref. 5). Additionally, *NIN* produced an alloy chemically similar to the Soviet alloy VN-10. This formulation, Nb-35Ti-5Al-4V-0.5Zr-0.05C (wt%), achieved a promising blend of solid-solution and carbide dispersion strengthening (Ref. 25).

Recent global intellectual property trends show that China is establishing absolute dominance in the research, development, and industrialization of LDNb alloys and their coatings (Refs. 24, 26 to 31). China's current R&D strategy focuses on using advanced vacuum melting and hot working capabilities to optimize alloy microstructure and performance. Using these methods, Chinese innovators successfully increased room-temperature elongation up to 24% to 27% while maintaining high tensile strengths greater than 900 MPa. There is growing evidence that the Chinese have mastered stamping, spin forming, and coating of LDNb alloys for aerospace applications (Refs. 5).

In the US today, Nb alloy C-103 (Nb-10Hf-1Ti, wt%) is the state-of-the-art commercial Nb alloy used in liquid rocket engine combustion chambers, radiatively cooled rocket nozzles, and jet engine afterburner flaps operating between 1,200 to 1,400 °C (Refs. 2 and 32). Developed jointly by Wah Chang Corp. (presently ATI Inc.) and Boeing Co. in the 1960s for space propulsion, C-103 uses Hf as the primary solid-solution strengthening element (Ref. 1). While C-103 is reliable, it is limited by its high density (8.85 g/cc) and low yield strength (~300 MPa at room temperature). The LDNb system offers a promising alternative for next-generation engines because it provides a 25% reduction in density and a three-fold increase in room-temperature yield strength (Ref. 21).

However, these LDNb alloys have a lower solidus temperature (~1,750 to 1,900 °C compared to ~2,300 °C for C-103). And they still must also be protected by advanced coatings to prevent oxidation at high temperatures (Refs. 21 and 33). Because of these factors, current research limits the use of LDNb components to temperatures below 1,200 °C (Refs. 2). Without surface protection, LDNb alloys undergo severe oxidation in air at temperatures above 800 °C. Adding an anti-oxidation coating extends this temperature range to ~1,300 °C (Refs. 13 and 34). Slurry-applied fused silicide coatings, including the US-developed R512A (Si-20Cr-5Ti, wt%) and R512E (Si-20Cr-20Fe, wt%), remain the benchmark. These coatings produce a multilayer diffusion zone that protects the underlying component by forming sacrificial SiO_2 and complex oxides (Refs. 13 and 34).

Even though these coatings provide environmental protection, they require high firing temperatures (1,350 to 1,450 °C) that cause recrystallization and coarsening in Nb alloys. These temperatures significantly exceed the 880 to 1,000 °C recrystallization threshold of LDNb alloys, which triggers rapid grain growth that eliminates desirable fine-grained microstructures. For example, recent testing of thin-sheet LDNb alloy specimens coated with a R512A slurry demonstrated a 29.5% drop in yield strength and a severe 54.6% reduction in elongation at failure (Ref. 34). Therefore, developing coating application cycles that restrict microstructural coarsening and reduce elemental diffusion are primary challenges before LDNb alloys can be widely used in next-generation aerospace propulsion systems (Refs. 5 and 34).

Recent breakthroughs in laser powder bed fusion (L-PBF), a type of metal additive manufacturing (AM), allow engineers to add strengthening nanoparticles directly into metal alloys during printing. This process makes it easier to create materials for extreme environments. For example, NASA's GRX-810 is an advanced NiCoCr-based oxide dispersion strengthened (ODS) alloy. It features nanoscale yttria (Y_2O_3) particles uniformly distributed throughout the printed metal to improve elevated temperature performance (Ref. 35). To make this alloy, nanoscale oxides are coated onto pre-alloyed metal powders using a high-energy acoustic mixing process. This approach does not disturb the original sphericity of the powders and replaces traditional, expensive, and complex mechanical alloying approaches. Following 3D-printing, high-resolution electron microscopy has shown that this fine dispersion of nano-oxides successfully pins dislocations, creating stable defect networks that obstruct dislocation motion. Consequently, when compared to conventional AM superalloys, GRX-810 shows a two-fold improvement in tensile strength, an over 1,000-fold longer high-temperature creep life (time to 1% strain), and a two-fold improvement in cyclic oxidation performance up to extreme temperatures (~1,200 °C) (Ref. 35).

L-PBF printing with nanoparticle-coated powder provides a new way to prevent the flaws that typically limit LDNb alloys. Historically, these alloys suffered from the major problems described earlier: loss of strength due to microstructural instability and rapid grain growth above 1,000 °C, and poor compatibility with protective coatings due to high firing temperatures. Inspired by the recent success of GRX-810, this work proposes incorporating yttria nanoparticles to enhance the mechanical behavior and microstructural stability of an LDNb alloy. Past research on oxide dispersion strengthening of Nb alloys concluded that oxide particle coarsening rates were excessively high to serve as high temperature dislocation barriers (Refs. 11 and 36). However, until recently (Refs. 26 and 37), the use of yttria as the candidate dispersoid in Nb was not studied extensively. Yttria is highly stable at elevated temperatures ($-\Delta G_{1500°C}$: 1482 kJ/mol), and Y has a lower diffusivity in a Nb matrix ($D_{1500°C}$: 0.001 cm^2/sec) compared to common reactive metal additions like Zr and Hf (ZrO_2/HfO_2 $-\Delta G_{1500°C}$: ~400 kJ/mol, Zr/Hf $D_{1500°C}$: ~0.46 cm^2/sec) (Ref. 36).

By creating a stable, ultra-fine dispersion of yttria particles within the BCC matrix, an ODS LDNb alloy should inhibit recrystallization and grain coarsening during high-temperature service (850 °C or greater) (Refs. 35 and 36). Furthermore, the nano-dispersoids act as small pegs that improve the adherence of the growing oxide scale, which helps to reduce thermal expansion mismatch and suppress the spallation that leads to linear oxide growth kinetics (Ref. 35). In addition, by restricting high-temperature dislocation motion, the yttria particles may prevent the severe strength drop above 1,000 °C (Ref. 35). Using AM to add an oxide dispersion to LDNb alloys creates a new way to manufacture Nb components that are both lighter and more thermo-mechanically stable.

This study evaluates a novel LDNb alloy with a nanoscale yttria dispersion produced via L-PBF. The investigation explores whether this material can replace Ni-based alloys or even traditional Nb-based alloys like C-103. The goal is to meet the high-temperature demands of aerospace applications while lowering the cost and weight of printed refractory metal components. The work will benchmark the novel LDNb material's elevated-temperature mechanical performance against state-of-the-art Ni-based superalloys and legacy LDNb alloys. The results will show whether this new alloy successfully bridges the performance gap, especially for retaining strength at temperatures above 850 °C and resisting creep.

To address the reality that procuring lab-scale quantities of custom Nb alloy spherical powder for L-PBF is exceptionally difficult, this work uses an alternative strategy. The starting feedstock is created by blending two widely available commercial powders: Nb521 (Nb-5W-2Mo-1Zr, wt%) and Ti64 (Ti-6Al-4V, wt%). While this blended-powder approach bypasses procurement barriers, in-situ alloying during printing introduces other challenges due to differences in powder melting temperatures (~2,470 °C for Nb521 and ~1,660 °C for Ti64) and densities (Ref. 35).

2.0 Experimental Methods

2.1 Materials

The feedstocks used in this study were spherical niobium alloy Nb521 (Nb-5W-2Mo-1Zr, wt%), spherical titanium alloy Ti64 (Ti-6Al-4V, wt%), and angular high-purity (99.95%) chromium (Cr) powders. The initial Nb521 feedstock had a nominal particle size distribution (PSD) of 15 to 53 μm, which was subsequently sieved using a 400-mesh (37 μm) screen to restrict the maximum particle diameter to 37 μm. This powder size reduction was strategically necessary to balance the higher melting temperature of the Nb alloy. By minimizing the volume and thermal mass of individual Nb-alloy particles relative to the Ti-alloy powder, uniform melting at a given laser power density is promoted, ultimately allowing for a more homogeneous melt pool during L-PBF. The spherical Ti64 feedstock conformed to *ASTM* B348-13 Grade 5 specifications with a PSD of 15 to 45 μm. The angular Cr powder was sieved through a 635-mesh (20 μm) screen to ensure a maximum particle size around 20 μm. Restricting the Cr particle size was necessary both to mitigate the adverse effects of its angular morphology on powder flowability and to ensure uniform distribution throughout the material during L-PBF consolidation. High-purity (99.999%) yttria nanoparticles with an average particle size of <100 nm were added for oxide dispersion strengthening.

2.2 Powder Processing

Initial modeling explored several target compositions that aimed to match the chemistry of historical alloys like VN-10 (30-34 wt% Ti, 7-10 wt% Al, 4-6 wt% V or Cr) (Ref. 4). However, powder blending was constrained by the fixed elemental ratios within the pre-alloyed Nb521 and Ti64 feedstocks. To achieve an oxygen-tolerant composition with sufficient Al (> 5 at%), while balancing the amount of

added Ti to remain comparable to legacy alloys (25-35 wt% Ti), a 62:35:3 weight ratio of Nb521:Ti64:Cr was established. The constituent metallic powders were first blended to ensure homogeneity. The calculated chemical composition of the final blended mixture is provided in Table 1, yielding approximately 31.5 Ti, 3.0 Cr, and 2.2 Al (wt%).

Following blending of the metallic powders, the yttria nanoparticles were "coated" onto the blended feedstock via a resonant acoustic mixing process (Ref. 35). An yttria content of sub-1 wt% was selected because additions within this range did not degrade powder flowability or narrow the L-PBF processing window. The final Nb521-Ti64-Cr-Y_2O_3 feedstock's particle size distribution was measured using a *Horiba LA-950V2* laser scattering PSD analyzer and had a D_{10} of 17.7 μm and a D_{90} of 42.5 μm. Secondary electron (SE) micrographs of the final mixed powder including energy-dispersive X-ray spectroscopy (EDS) mapping to verify homogeneity of the mixture and higher magnification images detailing the smaller Cr angular powder and yttria nanoparticles decorating the spherical Nb- and Ti-based powders are shown in Figure 1.

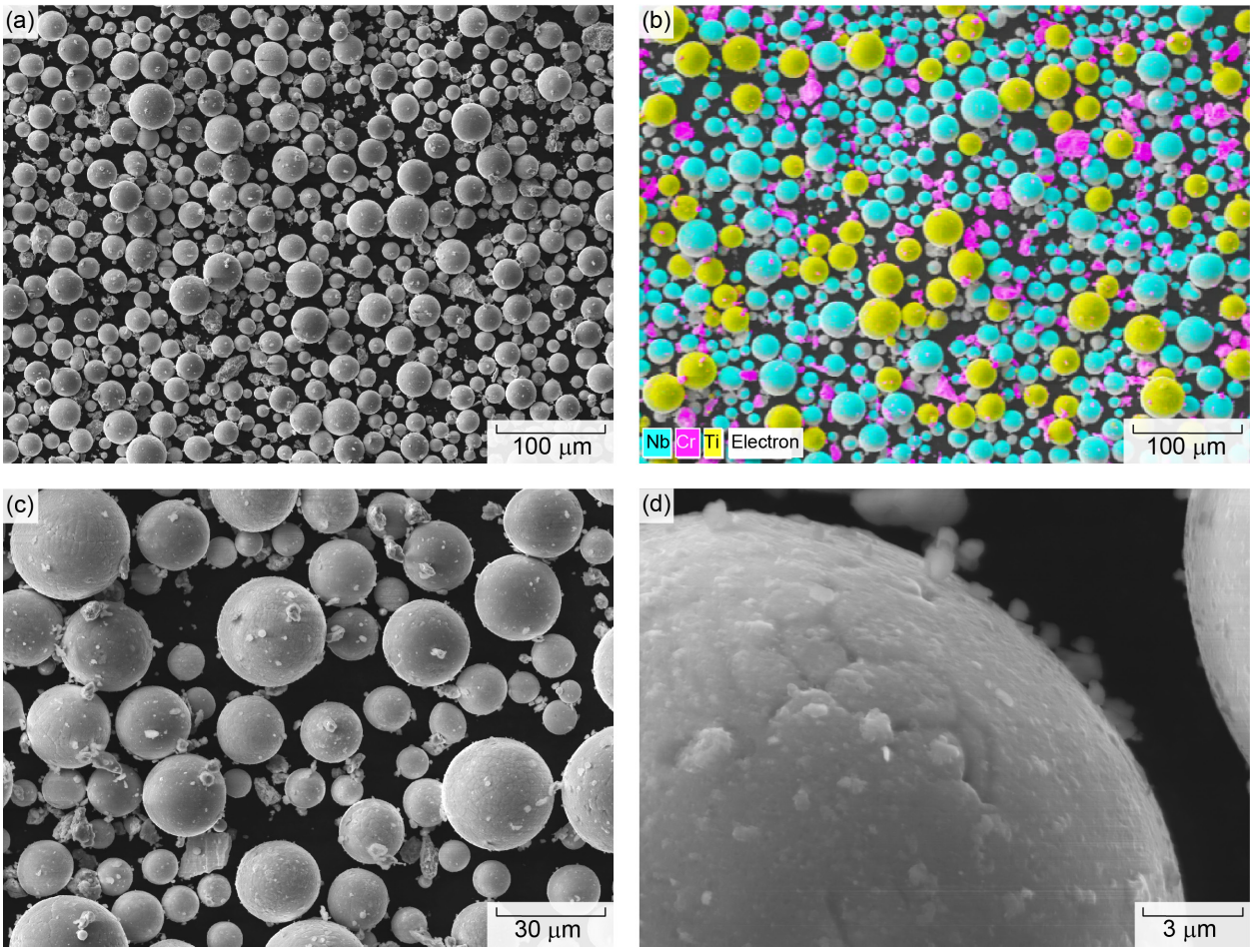

Figure 1. SE micrograph of the blended Nb521-Ti64-Cr-Y_2O_3 powders (a, c), SEM-EDS layered micrograph of the blended powders (b), higher magnification SE micrograph of the blended powders (c), and SE micrograph of the Y_2O_3 nanoparticles on the surface of the spherical powders (d)

2.3 Additive Manufacturing and Post-Processing

L-PBF consolidation was performed using an *EOS M100* system equipped with a 200 W Yb:YAG fiber laser (λ = 1,064 nm, 40 µm Gaussian spot diameter). To prevent oxidation during printing, the build chamber was continuously purged with ultra-high purity (UHP) argon to maintain an oxygen concentration below 10 ppm. One sub-size pin-loaded creep blank with nominal dimensions of 48.26 × 7.62 mm, two sub-size shoulder-loaded tensile blanks with dimensions 31.5 × 10 mm, and six oxidation blanks with dimensions 12 × 12 mm were arranged on a Ti64 build plate oriented 10° askew relative to the recoater blade travel direction (Figure 2(a)) and printed to a height of 18 mm. Although L-PBF used process parameters (laser power, scan speed, and hatch spacing, etc.) derived from a comprehensive optimization campaign to maximize the relative density of the consolidated material, there was a significant number of lack-of-fusion defects throughout the as-built microstructure (Figure 2(c)). And despite sieving the Nb521 particles to a maximum diameter of 37 µm, a chemically homogenous melt pool was not achieved. The micrographs in Figure 2 (c and d) show unmelted Nb521 powder throughout the build creating regions enriched in either Nb or Ti.

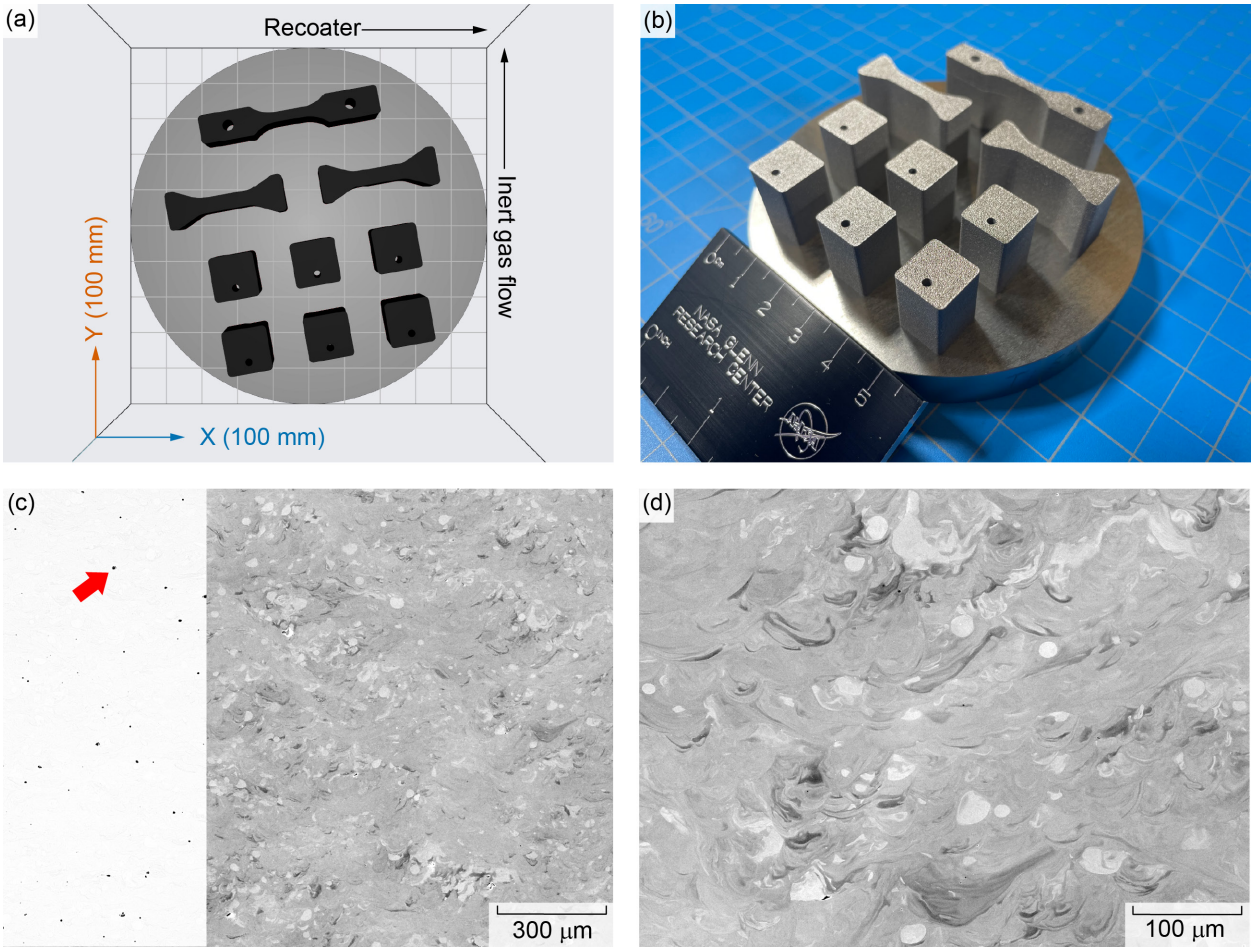

Figure 2. Schematic of the L-PBF build layout (a), image of the completed L-PBF build (b), combination overexposed optical micrograph (left) / SE micrograph (right) of the as-built microstructure with red arrow identifying lack-of-fusion defects (c), and higher magnification SE micrograph with “white” particles consisting of unmelted Nb521 (d).

Following L-PBF, the build was wrapped in tantalum (Ta) foil and was subjected to a high-vacuum ($<7\times10^{-4}$ Pa) heat treatment (VHT) at 1,400 °C for a hold time of 1 hr to homogenize the microstructure. This temperature was chosen after a series of VHT trials showed that temperatures below 1400 °C had insufficient mobility to ensure the Ti and Cr were present throughout the entirety of the metal matrix. However, even the 1,400°C/1 hr homogenization treatment left regions slightly enriched in either Nb or Ti. EDS line scans of the as-built and 1,400 °C VHT parts and their respective locations on an EDS map of the microstructure are shown in Figure 3.

After VHT, Mo-wire electrical discharge machining (EDM) was used to slice the pin-loaded creep specimens to a thickness of 2 mm, the sub-size shoulder-loaded tensile specimens to a thickness of 1.5 mm, and the oxidation specimens to a thickness of 3 mm. The oxidation testing results will not be reported on in this work. As a final preparatory step, the surfaces of the creep and tensile specimens were ground with 320-grit SiC paper to ensure a uniform surface finish on all sides of the gauge section. The density of an oxidation specimen (used as a "witness coupon") was measured using the Archimedes (hydrostatic weighing) method using deionized water as the submersion fluid to be 6.73 g/cc. And the chemical composition of the witness coupon was measured using SEM-EDS for the bulk elements and *LECO* combustion analysis for the trace elements (Table 1).

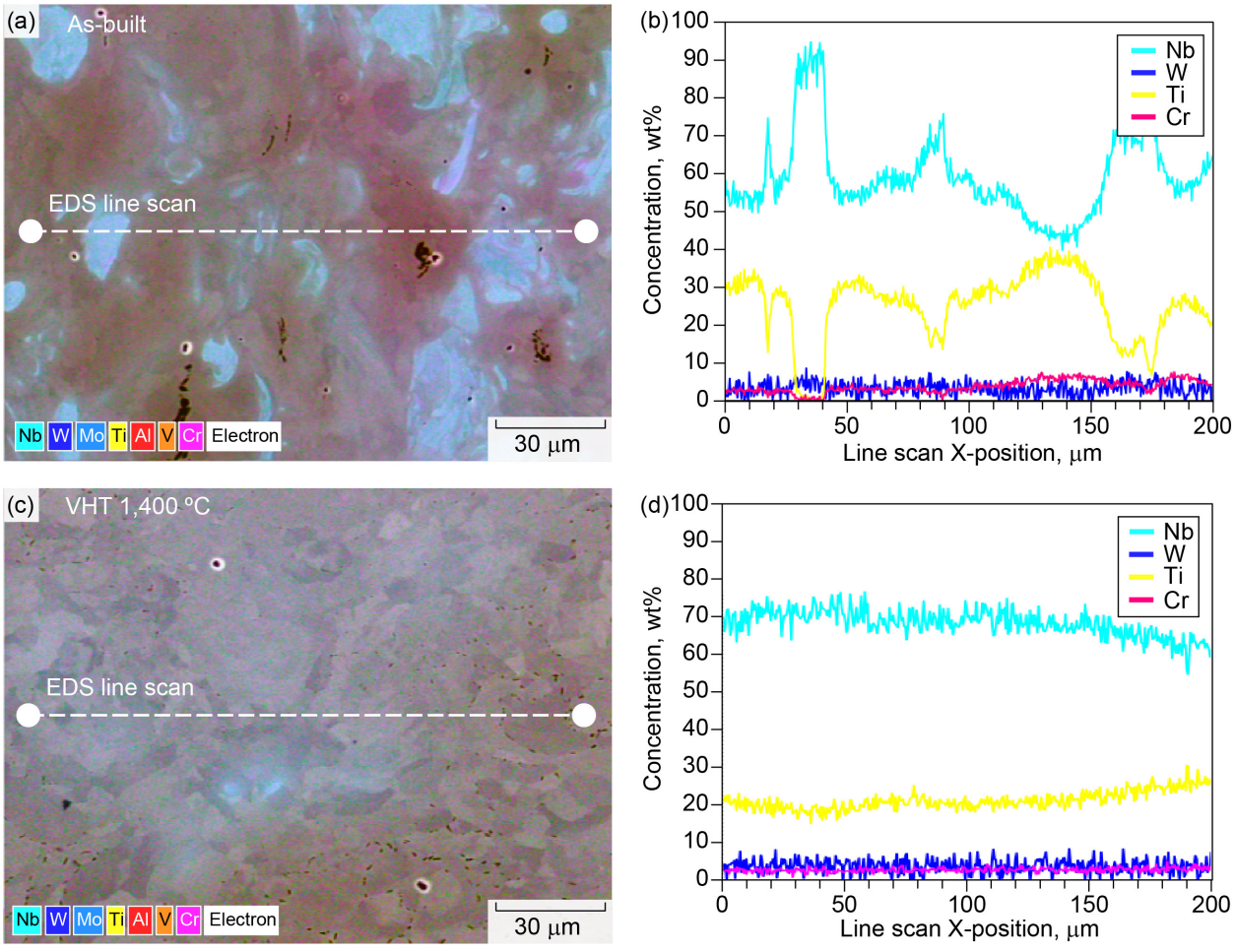

Figure 3. EDS layered micrograph with line scan location (a) and EDS line scan (b) of the as-built material; EDS layered micrograph with line scan location (c) and EDS line scan (d) of the 1,400 °C VHT material.

2.4 Mechanical Testing

To evaluate the material's elevated-temperature mechanical response while minimizing interstitial contamination, uniaxial tensile tests were conducted up to 1,300 °C in an inert argon environment within an *Instron* Electro-Thermal Mechanical Testing (ETMT) system. The ETMT chamber was pumped down to a vacuum of $<1\times10^{-4}$ Pa and then backfilled with UHP argon to a partial pressure of $\sim5\times10^{4}$ Pa prior to testing. Heating was achieved via direct electrical resistance (Joule heating), establishing a localized hot-zone (±20 °C of the target temperature) approximately 4 mm in length centered on the specimen gauge length. Temperature verification and closed-loop feedback control were maintained using a multi-wavelength pyrometer focused on the center of the gauge section. Strain was captured via two-dimensional digital image correlation. Prior to testing, a high-contrast, high-temperature speckle pattern was applied to the specimen surface. Images were acquired through a vacuum-rated optical port and processed using *VIC-Guage* software. Specimens were pulled at a programmed constant strain rate until at least 5% strain was reached. However, due to slight differences in hot-zone lengths the actual strain rate ranged from 2.1×10^{-4} s^{-1} to 3.1×10^{-4} s^{-1} with increasing temperature.

Complementary elevated-temperature stress-rupture testing was performed in ambient air at 1,093 °C to evaluate creep resistance in an oxygen-containing environment. Tests were executed on a custom "rapid" stress-rupture setup designed for rapid screening of high-temperature materials. The system is based on an *Applied Test Systems* dead-weight lever-arm creep frame. Specimens were heated within a three-zone resistance furnace to ensure thermal uniformity along the gauge length. Temperature monitoring and zone regulation were managed via Type-K thermocouples affixed near the specimen gauge. A constant predetermined dead-weight load corresponding to initial axial stresses ranging from 20.7 to 51.7 MPa were applied. The furnace is then turned on and ramps at a rate of ~25 °C/min to the target temperature of 1,093 °C. The total time-to-failure (rupture life) inclusive of the heat up ramp was logged upon specimen fracture detected via an integrated switch.

2.5 Metallographic Sample Preparation and Microscopy

Metallurgical specimens were sectioned from the as-fabricated tensile geometries. The extracted samples were hot-mounted in a conductive thermoset polymer, planar ground with progressively finer silicon carbide (SiC) abrasive paper, and polished to a 1 μm finish using diamond suspensions. Final surface preparation was achieved using a vibratory polisher with a 50 nm colloidal silica slurry to produce a deformation-free surface.

Microstructure and phase morphology were characterized using a *Tescan MAIA-3* field emission gun scanning electron microscope (FEG-SEM). Local chemical composition and secondary phase identification were evaluated via energy-dispersive X-ray spectroscopy (EDS) on targeted regions of interest. All electron microscopy observations were confined to the XZ-plane relative to the L-PBF build orientation depicted in Figure 2.

3.0 Results and Discussion

3.1 Chemical and Microstructural Analysis

The measured chemical composition of the Nb521 powder, Ti64 powder, and L-PBF consolidated and vacuum heat-treated LDNb-ODS material alongside the calculated chemical composition of the blended 62:35:3 LDNb feedstock is provided in Table 1. The ~6.7 wt% shift from the calculated blended feedstock composition (31.5 wt% Ti) to the L-PBF material (24.8 wt% Ti) was caused by Ti loss during the printing process. The Ti64 powder contained larger particles (up to 45 μm) than the Nb521 powder

(up to 38 μm). The recoater blade was more likely to push oversized Ti64 particles compared to Nb521 particles into the overflow bin instead of depositing them onto the powder bed. Also, because Ti64 (~4.43 g/cc) is nearly half as dense as Nb521 (~8.85 g/cc), the lighter Ti64 particles were more easily blown away by the inert shielding gas or sucked into the laser vapor plume and kicked out as spatter (Refs. 38 and 39). Additionally, the melt pool reached temperatures where Ti may have evaporated due to its lower boiling point (~3,287 °C vs. ~4,744 °C for Nb) (Ref. 38). To compensate for Ti loss in future builds, the initial mixture should be over-alloyed with Ti64.

The oxygen content of the LDNb-ODS L-PBF material (0.124 wt%) is considerably higher than the allowable oxygen in most commercial Nb-based alloys which typically require less than 300 ppm (<0.03 wt%). Provided all the added Y_2O_3 was incorporated into the printed material, only ~200 ppm of oxygen can be attributed to the oxide nanoparticles. Therefore, over 0.1 wt% of the oxygen content came from the starting feedstocks (fine PSD with increased surface area) and/or was picked up during the L-PBF process. However, the alloy developed by Sikka and Loria in 1997 was produced with a similar 0.116 wt% oxygen level (Refs. 21).

Electron micrographs of the microstructure at various magnifications alongside EDS mapping of a region of interest is shown in Figure 4 for the fully processed material. The average grain size was determined via the circular intercept procedure (Hilliard method) in accordance with ASTM E112 (Ref. 40). Using a 100 μm diameter test circle across three fields of view (204 intercepts), the mean linear intercept length was measured at 4.62 μm. This grain structure is exceptionally fine; even compared to microstructures typically observed in L-PBF consolidated alloys, where rapid solidification cooling rates (10^5 to 10^6 °C/s) suppress grain growth and promote refinement (Refs. 2, 13, and 41).

Table 1. Chemical Composition (wt%) of Spherical Powder Feedstocks, Blended Powder Feedstock, and L-PBF Consolidated and Vacuum Heat-treated Material

Element	Nb521 Powder	Ti64 Powder	LDNb 62:35:3 Blend (Calc.)	LDNb-ODS L-PBF & VHT
Nb	Balance	-	Balance	Balance
Ti	-	Balance	31.5	24.8
Cr	-	-	3.0	3.2
V	-	3.7	1.3	1.2
Al	-	6.4	2.2	1.6
W	5.0	-	3.1	3.7
Mo	1.6	-	1.0	0.9
Zr	1.3	-	0.8	0.5
Y	-	-	-	-
O	/	/	/	0.124
N	/	/	/	0.023
C	/	/	/	0.007

"-" = not detected,
"/" = not measured

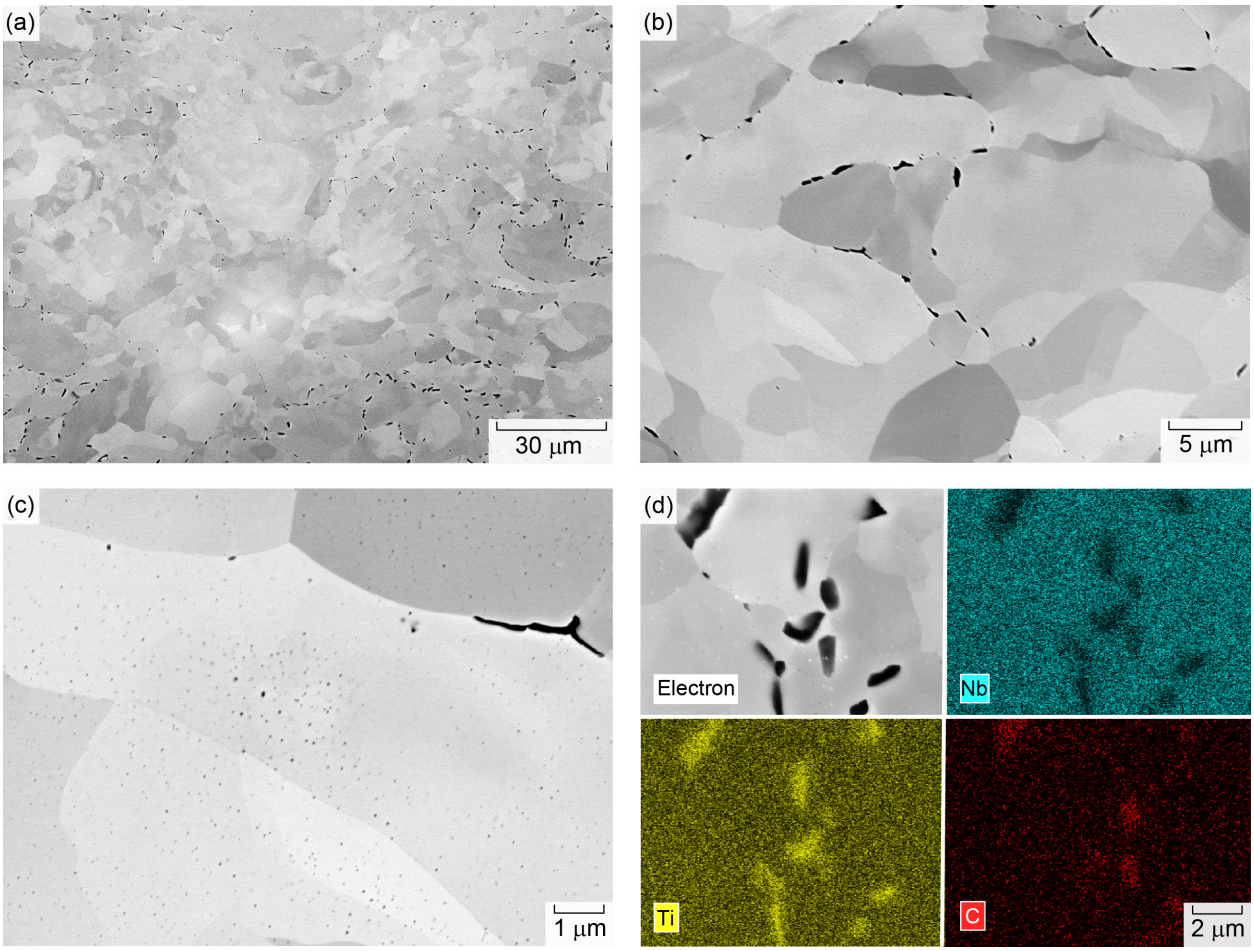

Figure 4. Lower magnification SE micrograph (a) and BSE micrograph (b) showing overall microstructure and grain boundary precipitates, higher magnification BSE micrograph (c) showing dispersed oxide nanoparticles, and EDS maps (d) identifying grain boundary precipitates and Ti-rich carbides or carbonitrides

Grain boundary precipitates were observed in the regions of the microstructure that were enriched in Ti. SEM-EDS mapping of the precipitates confirmed that the intergranular phases are Ti-rich. Spatial co-localization of Ti with carbon (and minor concentrations of nitrogen) indicates that these precipitates may be Ti-rich carbides or carbonitrides (Ti(C,N)). Image analysis of the precipitates determined a mean length (Major axis) of 0.81 μm, a mean width (Minor axis) of 0.28 μm, and an average aspect ratio between 2.5 and 3.2. The presence of these Ti(C,N) precipitates along the grain boundaries may contribute to improvement in high-temperature creep resistance by pinning the boundaries and preventing grain boundary sliding during thermal exposure (Refs. 35).

Although best characterized using transmission electron microscopy techniques, the oxide dispersion was measured on high magnification backscattered electron (BSE) micrographs that were processed and thresholded in *ImageJ* to isolate only the oxide particles. The yttria dispersoids exhibit a highly uniform nanoscale size distribution with a calculated mean equivalent circular diameter of 31.4 nm ± 11.5 nm determined via image analysis. The low standard deviation in diameter relative to the mean, paired with a tightly grouped aspect ratio of 1.48 and a high average roundness of 0.71, is indicative of a fine population of strengthening particles. This uniform and nanoscale size distribution is optimal for preventing intragranular dislocation motion at elevated temperatures (Refs. 36).

3.2 Elevated Temperature Tensile Testing

The results of the elevated temperature tensile testing including elastic modulus (E), 0.2% offset yield strength (YS), and ultimate tensile strength (UTS) are shown in Table 2. As YS is not reported as often as UTS in old reports, the UTS versus temperature of the LDNb-ODS alloy is compared against C-103 (Nb-10Hf-1Ti, wt%), the Soviet alloy VN-10 (~Nb-41Ti-7Al-4V-1.5Zr-0.08C, wt%), the "3899-4" alloy disclosed in a patent by Jackson in 1994 (Nb-23.9Ti-3.4V-1.8Al-11.9Hf-0.6Zr-0.03C-3.2Sn, wt%, hereafter called Jackson94), and the "B-2" alloy developed by Sikka and Loria in 1997 (Nb-24.3Ti-2.4Al-3.8Cr-5.9V-2.7W-0.7Mo-0.8Hf, wt%, hereafter called Sikka97) in Figure 5 (Refs. 15, 16, 21, and 32).

Across the evaluated temperature range, the LDNb-ODS exhibits a classic thermal softening response characteristic of many BCC structural alloys (Ref. 2). Compared to alloy C-103, LDNb-ODS is significantly stronger (up to 2.5x) from room temperature to 600 °C. The UTS then drops to cross C-103 at approximately 850 °C and 300 MPa. At temperatures above 1,000 °C, C-103 dominates due to its heavy and higher-melting refractory matrix with slow-diffusing Hf solutes (Refs. 1 and 2).

Within the plotted low-density alloys, LDNb-ODS has intermediate temperature strength comparable to Sikka97 and Jackson94, but significantly lower than VN-10 (Refs. 15, 16, and 21). Note that the strength of the VN-10 alloy begins to fall about 100 °C higher temperature than the others, i.e., near 700 °C (Ref. 15). Starting at ~650 °C and 110 MPa, LDNb-ODS trails behind Jackson94 and remains the weakest LDNb alloy until it intersects with VN-10 at approximately 900 °C and 200 MPa. Despite their chemical compositions being similar, the more rapid decay of LDNb-ODS compared to the other low-density alloys is likely attributed to material processing (e.g., lack-of-fusion defects and microstructural inhomogeneity) (Ref. 2).

From a metallurgical perspective, the LDNb-ODS's deficit in elevated-temperature tensile performance is likely due to strain partitioning driven by chemical inhomogeneity. As the microstructure exhibits regions enriched with either Nb or Ti, during elevated-temperature uniaxial tension, strain would not distribute uniformly across the bulk material. Instead, strain preferentially localizes in the weaker, Ti-enriched zones. Thermally activated deformation mechanisms like dislocation climb, cross-slip, and grain boundary sliding become dominant in the Ti-enriched areas (Refs. 2, 10, and 14). Consequently, these regions reach their yield criterion before the Nb-enriched regions, which further concentrates stress and causes localized necking.

The specific YS (normalized by alloy density in g/cc) versus temperature of the LDNb-ODS alloy is plotted alongside tensile data for a precipitation strengthened Ni718, solid solution strengthened Ni625 and Ni230, and a medium entropy alloy GRX-810, in Figure 6 (Refs. 42 to 45).

Table 2. Uniaxial Tensile Mechanical Properties
of the L-PBF LDNb-ODS Material (XY-direction)

Temperature, °C	E, GPa	$YS_{0.2}$, MPa	UTS, MPa
20	108	733	1,005
550	112	570	791
800	94.7	222	346
950	75.6	102	140
1,100	40.5	48.1	62.4
1,300	24.7	19.4	29.0

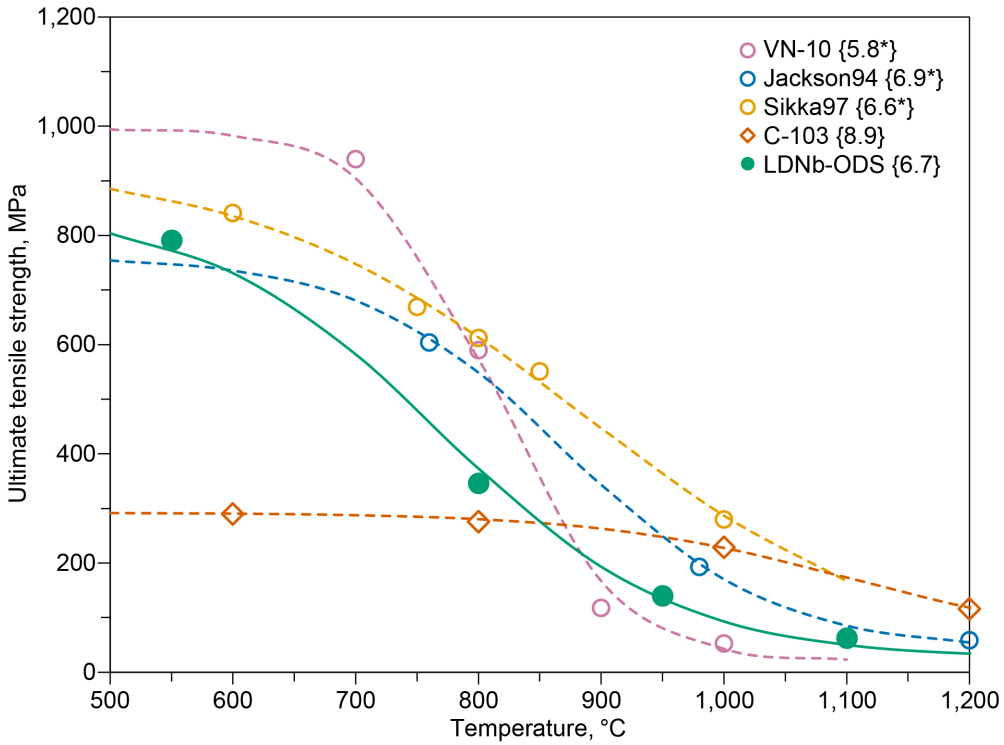

Figure 5. Ultimate tensile strength versus temperature of LDNb-ODS compared to low-density Nb alloys VN-10 (Ref. 15), Jackson94 (Ref. 16), Sikka97 (Ref. 21), and conventional Nb alloy C-103 (Ref. 32); {#} = alloy density in g/cc (* = estimated)

In the lower temperature range, Ni718 stands out with the highest specific yield strength (peaking above 100 MPa/(g/cc), while Ni625, Ni230, and GRX-810 form a lower plateau around 25 to 40 MPa/(g/cc). LDNb-ODS occupies a middle ground, maintaining a high specific yield strength of 60 to 85 MPa/(g/cc) that outperforms Ni-based alloys Ni625, Ni230, and GRX-810 up to approximately 800 °C.

Between 800 and 900 °C, a transition occurs. Ni718 and Ni625 undergo a steep drop in specific yield strength. LDNb-ODS also experiences thermal softening, but its rate of strength degradation is less severe than that of Ni718 (Ref. 42). By 870 °C, the performance of LDNb-ODS intersects with both Ni718 and Ni625, and by 950 °C, LDNb-ODS retains superior specific strength compared to both Ni718 and Ni625 (Refs. 42 and 43). Principles of Ni alloy physical metallurgy explain the drastic loss of strength in Ni718 as typical gamma-double-prime (γ″) and gamma-prime (γ′) coarsening, dissolution, or over-aging, alongside the onset of rapid dislocation climb and grain boundary sliding (Refs. 35 and 46). LDNb-ODS, while also experiencing softening due to thermally activated dislocation movement, maintains greater mechanical stability than Ni718 and Ni625, likely due to lower self-diffusion rates in its refractory Nb-rich matrix compared to the Ni matrix (Refs. 2 and 14).

At extreme temperatures above 1,000 °C, LDNb-ODS closely mirrors the moderate degradation slope of Ni230 and GRX-810, maintaining a competitive specific yield strength through 1,100 °C and extending out past 1,200 °C (Refs. 44 and 45). However, it is weaker than its ODS NiCoCr counterpart, GRX-810, despite having a higher melting point.

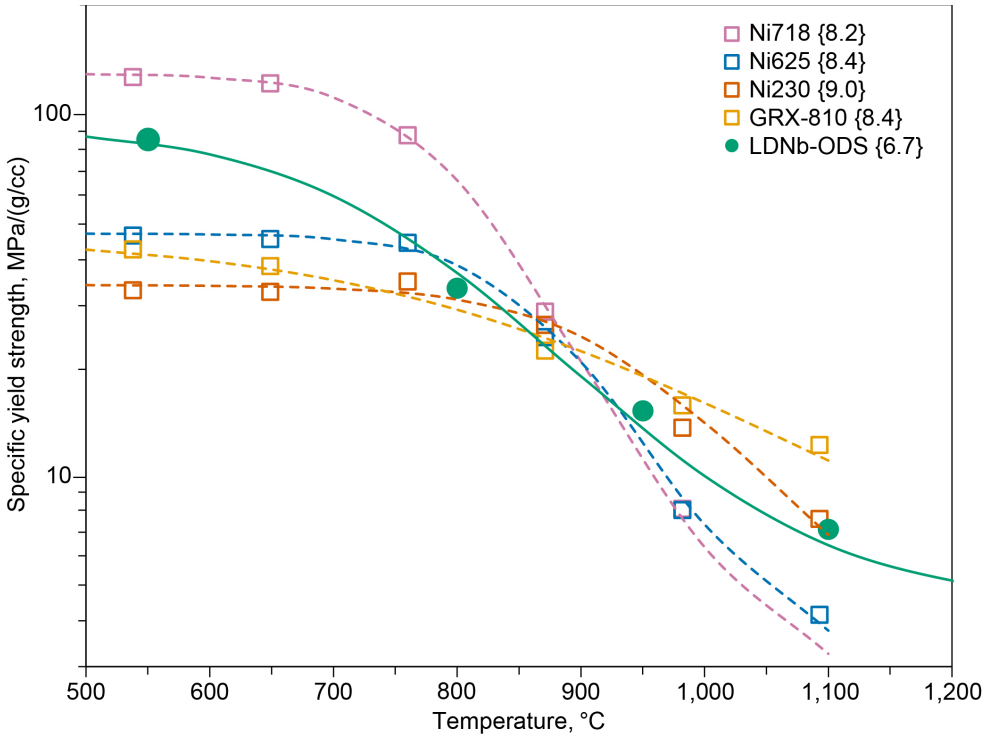

Figure 6. Specific 0.2% yield strength (normalized by alloy density in g/cc) versus temperature of LDNb-ODS compared to Ni alloys Ni718 (Ref. 42), Ni625 (Ref. 43), Ni230 (Ref. 44), and oxide dispersion strengthened NiCoCr alloy GRX-810 (Ref. 45); {#} = alloy density in g/cc

3.3 Stress Rupture Screening

The simplified stress-rupture test, known at NASA GRC as the "rapid-rupture" test, takes shortcuts in sample preparation, heats samples with the load already applied, and measures only the time to rupture. Because of these testing conditions, the data is only self-consistent and does not represent standardized material properties. Therefore, the plot in Figure 7(a) only compares materials tested on the NASA GRC “rapid” stress-rupture frames.

The data in Figure 7(a) shows the rapid stress-rupture lives of LDNb-ODS, GRX-810, Ni625, and C-103 at 1,093 °C. LDNb-ODS has better creep resistance than Ni625 and C-103, sustaining higher stresses for longer times. At stresses above 40 MPa, LDNb-ODS performs similarly to the NASA GRX-810 alloy. However, at the lowest tested stress of 20.7 MPa, the LDNb-ODS material failed at approximately 21.4 hr, while GRX-810 lasted ~190 hr. A LDNb-ODS specimen was coated with the R512E (Si-20Cr-20Fe, wt%) slurry-applied fused silicide coating (labeled LDNb-ODS+R512E in Figure 7(a)) and tested to evaluate the coating’s effect on oxidation resistance and rupture life. At a 20.7 MPa load, the coating increased the rupture life from 21.4 to 84.8 hr. This result confirms that oxidation, rather than mechanical creep alone, limits the long-term life of the LDNb-ODS alloy at 1,093 °C (Refs. 1 and 2).

When comparing C-103 to LDNb-ODS tested 20.7 MPa, the difference in appearance between the two alloys after cool-down (Figure 7(b)) highlights the role of Nb oxide formation in determining rupture life. C-103 underwent catastrophic oxidation, forming a pale yellow, highly fragile, non-protective scale characteristic of Nb_2O_5 that spalled into loose powder and delaminated fragments, leading to a reduction in load-bearing cross-section and failure (Refs. 10 and 33). In contrast, LDNb-ODS formed a denser, adherent, dark scale characteristic of a mixed TiO_2+Nb_2O_5 oxide that somewhat protected the underlying alloy, allowing the specimen to better maintain its structural cross-section and resulting in a ten-fold increase in rupture life (Refs. 10 and 33).

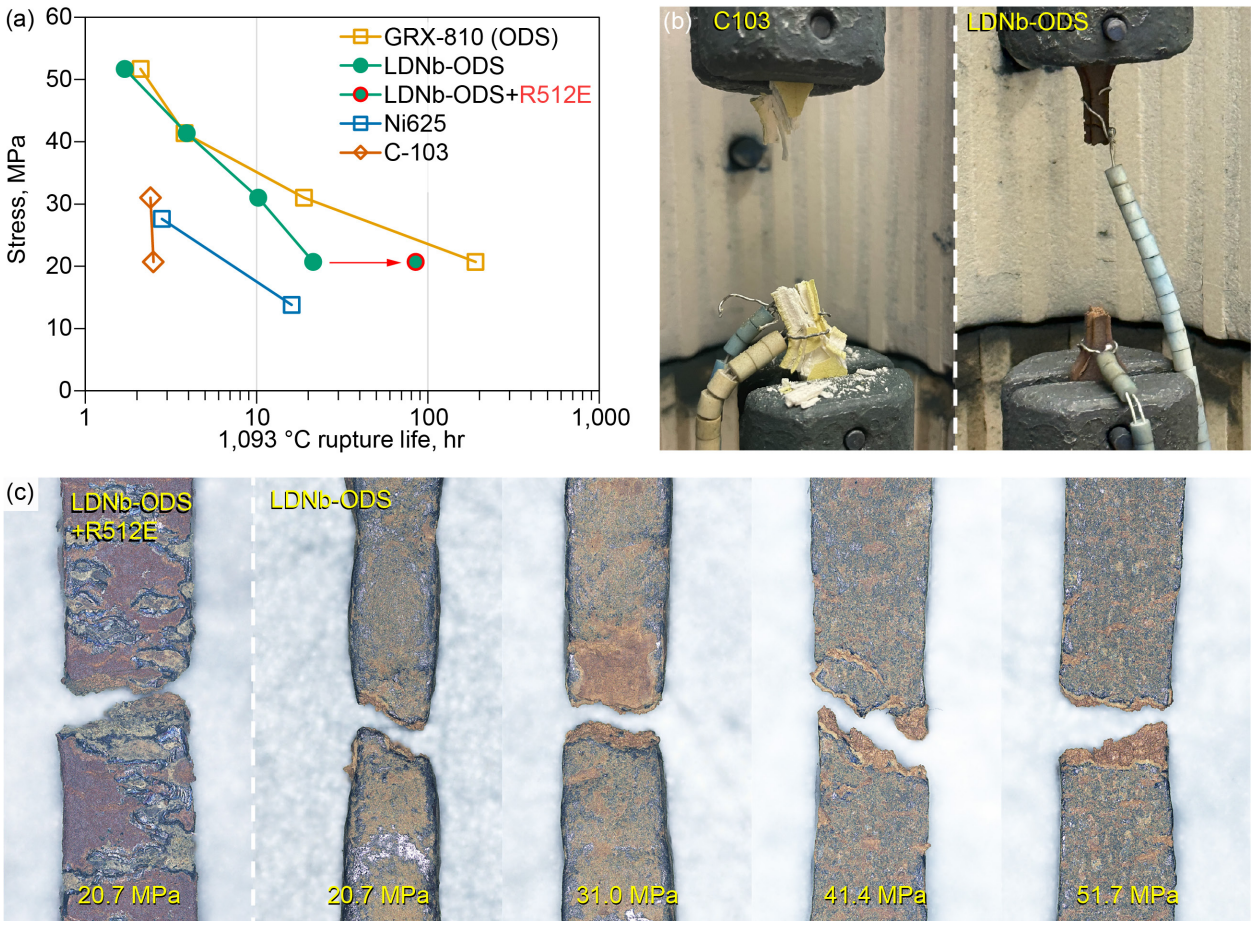

Figure 7. GRC-specific 1093°C rapid-rupture life of LDNb-ODS compared to GRX-810, Ni625, and C-103 (a), post rapid-rupture test images of the C-103 (left) and LDNb-ODS (right) specimens (b), and optical macrographs of the LDNb-ODS rapid-rupture fracture regions (c).

Images of the failure region for the LDNb-ODS alloy tested in both coated and uncoated conditions across the range of applied stress levels are shown in Figure 7(c). The uncoated series (20.7 to 51.7 MPa) have a progressively larger fracture surface area with increasing stress. The fracture and final load-bearing cross-sectional area of the R512E-coated specimen tested at 20.7 MPa more closely resembles the uncoated specimen tested at 51.7 MPa. Again, these visual observations confirm that oxidation-induced section loss accelerates failure at low stresses, and applying an environmental barrier coating successfully increases stress-rupture life (Refs. 1 and 33).

4.0 Conclusions

This study evaluated the feasibility of producing a novel, oxide-dispersion-strengthened low-density niobium alloy (LDNb-ODS) via L-PBF using a blended-powder feedstock strategy. By combining and consolidating Nb521, Ti64, and elemental Cr powders with nanoscale yttria, this work aimed to bridge the performance gap between conventional Ni-based superalloys and the heavier legacy Nb-based alloys for weight-sensitive, high-temperature (>850 °C) aerospace applications. The consolidated material was partially homogenized through a high-vacuum heat treatment at 1,400 °C and characterized via SEM-

EDS, elevated-temperature tensile testing up to 1,300 °C, and rapid stress-rupture testing at 1,093 °C. From the study, the following conclusions can be drawn:

1. Powder blending and L-PBF successfully consolidated the LDNb-ODS alloy and achieved a bulk density of 6.73 g/cc. However, the build was chemically inhomogeneous, had lack-of-fusion defects, and experienced preferential Ti loss during printing, which highlights the need to use pre-alloyed feedstock in future studies.
2. Vacuum heat treatment at 1,400 °C preserved an ultrafine grain structure (mean linear intercept grain size of 4.62 μm), stabilized by a uniform dispersion of yttria nanoparticles (31.4 ± 11.5 nm). Total oxygen content was held to 0.124 wt% (1,240 ppm), with nano-oxide additions accounting for ~200 ppm. These results demonstrate strong potential for mitigating grain coarsening during the high-temperature (1,350 to 1,450 °C) firing of environmental barrier coatings.
3. The LDNb-ODS alloy exhibited up to 2.5x higher UTS than C-103 from room temperature up to 600 °C. When normalized by density, LDNb-ODS maintained a high specific yield strength of 60 to 85 MPa/(g/cc) up to 800 °C, outperforming Ni-based superalloys Ni625, Ni230, and GRX-810. By 870 to 950 °C, LDNb-ODS surpassed both Ni718 and Ni625 as those alloys underwent rapid thermal softening, but did not outperform GRX-810 at 1,100 °C.
4. In rapid stress-rupture screening at 1,093 °C and 20.7 MPa, uncoated LDNb-ODS achieved a rupture life of 21.4 hr; significantly outperforming C-103, which suffered catastrophic oxidation. Applying a protective R512E fused silicide slurry coating increased LDNb-ODS's 20.7 MPa rupture life to 84.8 hr (a 4-fold increase), demonstrating that oxidation-induced section loss, rather than mechanical creep, is the primary driver of failure at lower stresses.

Overall, LDNb-ODS demonstrates potential as a lightweight, thermally stable alternative to Ni-based superalloys. But significant efforts are needed focusing on the use of pre-alloyed feedstock for chemical homogeneity, L-PBF parameter optimization to eliminate lack-of-fusion defects, and optimization of dispersoid additions to unlock the full mechanical potential of this alloy class.

References

1. J. Hebda, "Niobium Alloys and High Temperature Applications," Tech. Rep., Wah Chang Corp., Albany, OR, USA, 2001.
2. C. Frey, K. M. Mullin, J. Jankowski, L. H. Mills, N. R. Philips and T. M. Pollock, "A Perspective on the Historical and Contemporary Development of Refractory Alloys," *Metallurgical and Materials Transactions A,* vol. 56, no. 1, pp. 1-28, December 2025.
3. X. Zheng, R. Bai, D. Wang, X. Cai, F. Wang, M. Xia and J. Yu, "Research Progress of Refractory Alloys for Aerospace Applications," *Rare Metal Materials and Engineering,* vol. 40, no. 10, pp. 1871-1875, October 2011.
4. O. G. Ospennikova, V. N. Podyachev and Y. V. Stolyankov, "Refractory alloys for new technology," *Proceedings of VIAM,* vol. 10, no. 46, pp. 55-64, 2016.
5. B. Zhu, X. Wu, M. Wan, G. Zhao, Y. Cao, W. Luo, S. Li and J. He, "Research progress of high temperature niobium alloys for aerospace applications," *The Chinese Journal of Nonferrous Metals,* vol. 33, no. 1, pp. 1-26, January 2023.
6. M. R. Jackson, K. D. Jones, S. C. Huang and L. A. Peluso, "Response of Nb-Ti Alloys to High Temperature Air Exposure," in *Refractory Metals: Extraction, Processing and Applications*, K. C. Liddell, D. R. Sadoway, and R. G. Bautista, Eds. Warrendale, PA, USA: TMS, 1990.

7. M. R. Jackson and K. D. Jones, “Mechanical Behavior of Nb-Ti Base Alloys,” in *Refractory Metals: Extraction, Processing and Applications*, K. C. Liddell, D. R. Sadoway, and R. G. Bautista, Eds. Warrendale, PA, USA: TMS, 1990.
8. A. R. Stetson and A. G. Metcalfe, “Development of Coatings for Columbium Base Alloys: Part I - Basic Property Measurements and Coating System Development,” Air Force Materials Laboratory, Wright-Patterson Air Force Base, OH, USA, Tech. Rep. AFML-TR-67-139, 1967.
9. S. T. Wlodek, E. D. Weisert and P. M. Moanfeldt, “Columbium Base Alloy.” United States Patent 3 028 236, 3 April 1962.
10. K. D. Jones, “Microstructural and tensile property study of experimental niobium-titanium base alloys,” M.S. thesis, Dept. Mater. Eng., Rensselaer Polytechnic Inst., Troy, NY, USA, 1990.
11. V. G. Grigorovich and E. N. Sheftel, Dispersion Hardening of Refractory Metals, Moscow: Nauka Publishing House, 1980.
12. V. G. Grigorovich and E. N. Sheftel, “Physicochemical Fundamentals of the Development of Heat-Resistant Niobium Alloys,” *Metal Science and Heat Treatment (or original Russian: Metallovedenie i Termicheskaya Obrabotka Metallov),* vol. 24, no. 7, pp. 472-478 (or original Russian version pages: 23-29), July 1982.
13. X. Zheng, R. Bai, X. Cai, M. Xia, F. Wang, H. Liu, H. Wang and J. Yu, “Progresses of New Niobium Alloys,” *Materials China,* vol. 33, no. 9-10, pp. 586-593, October 2014.
14. I. S. Tsvilyuk and V. I. Pylnikov, “Creep and Stress Rupture Strength of 5VMTs Alloy Clad with VN7 Alloy,” *Strength of Materials (or original Russian translation: Problemy Prochnosti),* vol. 14, no. 10, pp. 1385-1388 (or original Russian version pages: 85-89), October 1982.
15. O. I. Eliseeva, V. I. Kalyandruk, A. A. Denisova and V. V. Shirokov, “Effect of Heat Treatment on the Structure, Phase Composition, and Mechanical Properties of VN-10 Alloy,” *Materials Science (or original Russian translation: Fiziko-Khimicheskaya Mekhanika Materialov),* vol. 29, no. 1, pp. 56-60 (or original Russian version pages: 62-68), January-February 1993.
16. M. R. Jackson, “NbTiAlCrHf Alloy and Structures.” United States Patent 5 366 565, 22 November 1994.
17. V. K. Sikka, S. Viswanathan and E. A. Loria, “Processing and Properties of Nb-Ti-Based Alloys,” in *Superalloys 1992*, S. D. Antolovich et al. Eds. Warrendale, PA, USA: TMS, 1992.
18. V. K. Vasudevan, K. J. Leonard and J. C. Mishurda, “A Study of the Kinetics of Phase Transformations in Nb-Ti-Al Alloys,” Univ. of Cincinnati, Cincinnati, OH, USA, Tech. Rep., 2000.
19. K. S. Chan, “A Computational Approach to Designing Ductile Nb-Ti-Cr-Al Solid-Solution Alloys,” *Metallurgical and Materials Transactions A,* vol. 32A, pp. 2475-2487, October 2001.
20. K. J. Leonard, J. C. Mishurda and V. K. Vasudevan, “Phase equilibria at 1100 °C in the Nb-Ti-Al system,” *Materials Science and Engineering A,* Vols. 329-331, pp. 282-288, 2002.
21. V. K. Sikka and E. A. Loria, “Characteristics of a multicomponent Nb-Ti-Al alloy via industrial-scale practice,” *Materials Science and Engineering A,* Vols. 239-240, pp. 745-751, 1997.
22. E. A. Loria, “The processing-microstructure-property relationship for a multicomponent Nb-Ti-Al alloy,” *Materials Science and Engineering A,* vol. 271, no. 1-2, pp. 430-438, 1999.
23. J. Zheng, X. Hou, X. Wang, Y. Meng, X. Zheng and L. Zheng, “Isothermal oxidation mechanism of a newly developed Nb-Ti-V-Cr-Al-W-Mo-Hf alloy at 800-1200 °C,” *International Journal of Refractory Metals and Hard Materials,* vol. 54, pp. 322-329, 2016.
24. G. Zhao, X. Zhou, J. Zhang and K. Dong, “Preparation and antioxidation mechanism of Nb-Ti-Al based alloy protective coatings,” *Powder Metallurgy Technology,* vol. 35, no. 5, pp. 348-351, October 2017.

25. R. Bai, X. Zheng, Z. Li, X. Cai, F. Wang, D. Wang and J. Yu, “Precipitation strengthening mechanism of Nb-Ti-Al alloys,” *Procedia Engineering,* vol. 27, pp. 1241-1247, 2012.
26. L. Zhang, X. Chen, Y. Liu, X. Chen, M. Qin and X. Qu, “A method for preparing a niobium-based alloy with an ultrafine oxide dispersion phase.” China Patent 111 926 208 A, 13 November 2020.
27. F. Wang, R. Bai, X. Cai, M. Xia, H. Liu, H. Wang and W. Bai, “A method for preparing a low-density Nb-Ti-Al-V-Zr-C niobium alloy bar.” China Patent 114 855 107 A, 5 August 2022.
28. J. Yu and L. Li, “A lightweight niobium alloy material for cryogenic environments and its preparation method.” China Patent 115 287 515 A, 4 November 2022.
29. P. Li, G. Hu, Z. Zhao, J. Li and C. Dong, “Method for adding rare earth elements to high-temperature niobium alloys.” China Patent 119 162 477 A, 20 December 2024.
30. K. Shobu, H. Hirai, T. Tabaru, H. Ueno and A. Kitahara, “High temperature oxidation resistant alloy materials and method of producing the same.” United States Patent 6 303 075 B1, 16 October 2001.
31. G. Wang, M. Li, B. Ma, S. Xiao, Y. Zhang, J. Guo and H. Chao, “A high-strength niobium alloy bar and its preparation method.” China Patent 118 048 540 A, 17 May 2024.
32. E. Brizes, J. Milner, E. Young-Dohe, A. Garg and R. Noebe, “Effect of Temperature on Tensile Properties of Laser Powder Bed Fusion Additively Manufactured Niobium Alloy C103,” *Metallurgical and Materials Transactions A,* vol. 56, pp. 928-941, March 2025.
33. R. A. Perkins, K. T. Chiang, G. H. Meier and R. A. Miller, “Effect of Alloying, Rapid Solidification, and Surface Kinetics on the High Temperature Environmental Resistance of Niobium,” Tech. Rep. LMSC-F352227, Lockheed Missiles & Space Co., Inc., Palo Alto, CA, USA, 1989.
34. G. Zhao, X. Zhou, B. Liang, X. Bai, Z. Cai and S. Yang, “Effect of silicide coating on mechanical properties of Nb-Ti-Al alloys,” *Powder Metallurgy Technology,* vol. 40, no. 6, pp. 494-498, December 2022.
35. T. M. Smith, C. A. Kantzos, N. A. Zarkevich, B. J. Harder, M. Heczko, P. R. Gradl, A. C. Thompson, M. J. Mills, T. P. Gabb and J. W. Lawson, “A 3D printable alloy designed for extreme environments,” *Nature,* vol. 617, pp. 513-518, May 2023.
36. D. L. Anton, D. B. Snow, L. H. Favrow and A. F. Giamei, “Dispersion Strengthening of High Temperature Niobium Alloys,” United Technologies Research Center, East Hartford, CT, USA, 1989.
37. X. Zhang, Z. Song, M. Shao and Q. Yan, “An oxide dispersion strengthened niobium alloy and its preparation method.” China Patent 118 326 219 A, 12 July 2024.
38. ASM International Handbook Committee, ASM Handbook, Volume 2: Properties and Selection: Nonferrous Alloys and Special-Purpose Materials, Materials Park, OH, USA: ASM International, 1990.
39. E. Brizes and J. Milner, A Comparison of Niobium Alloys C103 and Nb521, Cleveland, OH, USA, Tech. Rep.: NASA Glenn Research Center, 2025.
40. ASTM International, “Standard Test Methods for Determining Average Grain Size, ASTM Standard E112-13,” ASTM International, West Conshohocken, PA, USA, 2021.
41. Q. Li, L. Zhang, D. Wei, S. Ren and X. Qu, “Porous Nb-Ti based alloy produced from plasma spheroidized powder,” *Results in Physics,* vol. 7, pp. 1289-1298, 2017.
42. Haynes International, “Haynes 718 alloy,” Haynes International, Kokomo, IN, USA, Tech. Data Sheet, 2020.
43. Haynes International, “Haynes 625 alloy,” Haynes International, Kokomo, IN, USA, Tech. Data Sheet, 2020.
44. Haynes International, “Haynes 230 alloy,” Haynes International, Kokomo, IN, USA, Tech. Data Sheet, 2021.

45. National Aeronautics and Space Administration, “GRX-810 NASA Developed Data Sheet,” Tech. Rep., Washington, DC, USA, 2025.
46. R. C. Reed, The Superalloys: Fundamentals and Applications, Cambridge: Cambridge University Press, 2006.